ACS APPLIED MATERIALS & INTERFACES

Research Article

www.acsami.org

Role of Copper Sulfide Seeds in the Growth Process of $CuInS_2$ Nanorods and Networks

Jie Li, Mathieu Bloemen, Jürgen Parisi, and Joanna Kolny-Olesiak*

Energy and Semiconductor Research Laboratory, Department of Physics, Carl von Ossietzky University of Oldenburg, 26129 Oldenburg, Germany

Supporting Information

ABSTRACT: $CuInS_2$ nanorods and networks are interesting candidates for applications requiring efficient charge transport, such as solar energy conversion, because of the increased electrical conductivity in elongated or interconnected nanocrystals, compared to isolated, quasi-spherical ones. However, little is known about the growth mechanisms involved in the formation of this kind of nanostructures, yet. Here, $CuInS_2$ nanorods and networks were synthesized through a facile low-cost and phosphine-free method. Copper and indium sources were added together in the presence of oleylamine and oleic acid. Changing the amount of oleic acid present in the reaction solution influenced the reactivity of the monomers, and consequently, the size of copper sulfide seeds formed in situ after the injection of *tert*-dodecanethiol, serving as the source of sulfur. Two different growth mechanisms of $CuInS_2$ nanorods were observed, depending on the size of the copper sulfide seeds. Larger seeds (8 nm), which were generated with relatively small amounts of oleic acid, resulted in the formation of hybrid copper sulfide-copper indium disulfide nanocrystals as intermediates in the growth process of the nanorods, while smaller seeds (4 nm) obtained with relatively large amounts of oleic acid were gradually converted to copper indium sulfide nanorods. At longer reaction times, these nanorods formed network structures. The reaction between oleylamine and oleic acid at high temperature turned out to be the crucial factor to induce the attachment of nanorods to multipods and networks.

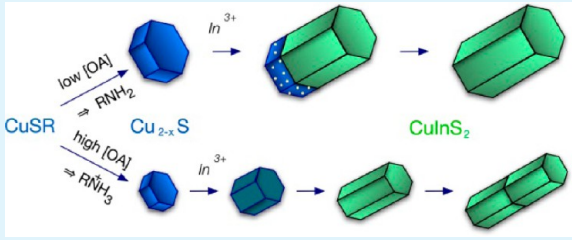

KEYWORDS: *copper indium disulfide, copper sulfide, hybrid nanostructure, shape control, colloidal synthesis, nanorods*

1. INTRODUCTION

Semiconductor nanocrystals (NCs) have attracted much attention over the past years as a novel class of materials with unique electronic and optical properties,[1−4] which make them interesting for applications, such as, biolabeling,[5] nanoelectronics, light emitting diodes, or photovoltaics.[6] $CuInS_2$ (CIS) is one of the most promising materials for solar energy conversion due to the direct band gap of approximately 1.5 eV which is well matched with the solar spectrum.[5,7−10] However, not only the absorption properties play an important role for a successful application in photovoltaics. Also the charge transport through the absorber material has a strong influence on the device performance. The electrical conductivity of nanomaterials strongly depends on their shape and is higher for elongated nanostructures compared to spherical particles. Therefore, shape control is particularly important, when synthesizing nanocrystals for application in solar cells. However, only a small percentage of the numerous studies devoted to the synthesis of pure CIS NCs demonstrated precise shape control.[9,11−14] In particular, our group has successfully synthesized monodisperse $Cu_{2-x}S$-CIS hybrid NCs and CIS nanoparticles with different shapes, for example, nanorods, hexagonal plates, or p-shaped particles.[13] The formation of hybrid $Cu_{2-x}S$-CIS nanostructures turned out to be the key to the successful shape control of CIS nanocrystals in our synthesis. Copper sulfide is a superionic conductor already at temperatures above 105 °C; while the anion lattice of this material maintains its solid state, the cations can move freely throughout the crystal.[15] Because of this high mobility of the cations within the anionic framework, copper sulfide can play a role of a catalyst in the growth of other semiconductor materials.[16] Although several examples of successful synthesis of nanocrystalline, shape-controlled semiconductors have been demonstrated during last years, which started with copper sulfide seeds and were based on copper sulfide containing hybrid nanostructures (Janus type particles) as intermediates,[11,13,17−24] the underlying growth process was not described in detail in most cases.[16] What is more, CIS particles, usually synthesized starting with copper sulfide seeds, are relatively large, so that no quantum size effect or shape dependent absorption could be observed in these CIS nanostructures.[13] Thus, it would be interesting to reduce the size of the copper sulfide seeds in order to decrease the thickness of the resulting CIS nanorods. However, many questions are still open, concerning, for example, the influence of the size, shape, and crystallographic structure of the copper sulfide seeds on the growth of the hybrid nanostructures.

Received: September 9, 2014
Accepted: October 27, 2014
Published: October 27, 2014

In the current work, we address one of these questions, namely, the influence of the size of the copper sulfide seeds on the growth process of CIS nanocrystals. We modified the reaction system from our previous work toward a lower cost and less toxic, phosphine-free synthesis approach. The particles are synthesized here in a mixture of oleylamine and oleic acid. This allowed us tuning the reactivity of the precursors and obtaining copper sulfide seeds with two different sizes. As a result, we observed two different growth mechanisms for the CIS nanocrystals, one involving $Cu_{2-x}S$-CIS hybrid NCs, the other based on a gradual conversion of copper sulfide into CIS nanocrystals. What is more, this modification of the synthetic method opens up the possibility for further morphological control by a secondary growth process. Shapes, which are not accessible with other methods, such as multipods and networks of CIS nanorods were, for the first time, successfully synthesized with our approach.

2. EXPERIMENTAL DETAILS

2.1. Chemicals. Copper(I) acetate (CuAc, 97%), 1-dodecanethiol (1-DDT, 98%), *tert*-dodecanethiol (*t*-DDT, 98.5%), oleic acid (OA, 90%) were purchased from Aldrich. Oleylamine (OLAM, 80−90%) and indium(III) acetate ($InAc_3$, 99.99%) were delivered from Acros and Alfa Aesar, respectively. All chemicals were used without further purification.

2.2. Synthesis of $CuInS_2$ Nanorods. In a typical procedure, 1.5 mmol copper acetate, 1 mmol indium acetate, and 3.2 mL (10 mmol) OA were mixed and subsequently dissolved in 10 mL oleylamine in a three-neck flask and stirred under vacuum at room temperature for 30 min. Afterward, the reaction system was heated to 240 °C (or 200 °C) under nitrogen flow. When the color of the solution turned from turbid green to slightly yellow, the mixture of 0.25 mL 1- dodecanthiol (1-DDT) and 2.5 mL *tert*-dodecanthiol (*t*-DDT) was rapidly injected into the solution. Small aliquots were taken out during different time intervals between 30 s and 1 h. Finally, the reaction system was cooled to room temperature, and the nanoparticles obtained were precipitated and washed by adding ethanol to remove residual thiols, acetates, and OA. The purified precipitate was then redissolved in hexane.

2.3. Synthesis of $CuInS_2$ Networks. $CuInS_2$ networks were obtained, when the amount of OA was increased to 16 mL (50 mmol). Because of the evolution of water, due to the reaction between OA and OLAM starting at 200 °C, no higher temperature could be reached, and the reaction was conducted at 200 °C. Aliquots were taken out of the reaction solution at different reaction time (varying between 30 s and 1 h) and the particles were isolated from unreacted precursors and byproducts of the reaction by precipitation in ethanol and redissolution in hexane.

2.4. Characterization. UV−vis spectra were obtained on a Varian Cary 100 Scan spectrophotometer. Transmission electron microscopy (TEM) images were acquired using a Zeiss EM 902A transmission electron microscope with an acceleration voltage of 80 kV. High resolution TEM (HRTEM) images were taken with a JEOL JEM-2100F microscope at 200 kV. Powder X-ray diffraction was obtained by wide-angle X-ray scattering using a PANalytical X'Pert PRO MPD diffractometer equipped with Cu Kα radiation. The samples were measured on low background silicon sample holders. The integral stoichiometry was obtained by the EDAX detector integrated into a FEI Quanta 200 3D scanning electron microscope. Stoichiometry of individual nanoparticles was analyzed with the EDX detector of the JEOL JEM-2100F microscope.

3. RESULTS AND DISCUSSION

CIS nanorods and networks were synthesized by a hot-injection method in oleylamine (OLAM) as solvent. We used copper(I) and indium(III) acetate as the sources of cations, while the thermal decomposition of *tert*-dodecanethiol (*t*-DDT),[13,25,26] provided the reaction solution with sulfur monomers. 1-dodecanethiol (1-DDT), present in the injection solution together with *t*-DDT (1-DDT/*t*-DDT = 1:10), is more stable and plays a role of a ligand for the resulting particles. Because of the different chemical properties of copper and indium cations (soft and hart Lewis acid, respectively), we applied not only 1-DDT (soft Lewis base), but also oleic acid (OA) (hard Lewis base) as stabilizer.

By varying the amount of OA, we could control the morphology of the resulting particles and influence their growth process. However, all the reactions described below have in common that the growth process of CIS nanocrystals starts with the formation of copper sulfide seeds. This indicates a higher reactivity of the copper compared to the indium monomers in our reaction solution. We attribute this to efficient coordination of the indium ions by OA and OLAM. This is supported by a comparison with literature showing a higher reactivity of indium precursors in the synthesis of CIS conducted in the presence of 1-DDT and absence of OA and OLAM.[5] Another factor facilitating the formation of copper sulfide particles is the presence of *t*-DDT. This thiol, as a soft Lewis base, can bind to copper cations; however, the resulting copper thiolate has a relatively low thermal stability. Our control experiments show that it can be decomposed to copper sulfide at temperatures below 100 °C (for comparison, copper thiolate generated from 1-DDT decays to Cu_xS above 230 °C).[27]

In most cases, the composition of the resulting particles differs from exact $CuInS_2$ stoichiometry; however, we refer to all of them as CIS, for the sake of simplicity. In the following, results obtained in reactions starting with the formation of 8- and 4-nm copper sulfide seeds (using 10 or 50 mmol OA, respectively) are presented, and the different growth mechanisms are discussed (Sections 3.1 and 3.2, respectively). In the last part of the Result and Discussion section (3.3) we address the reason for the dependence of the size of the copper sulfide seeds on the OA concentration in the reaction solution, based on ^1H and ^{13}C NMR measurements.

3.1. Growth Process of CIS Nanorods Starting with In Situ Formed 8 nm Copper Sulfide Seeds. Reactions with 10 mmol oleic acid were conducted at two different temperatures. At 240 °C, the formation of the nanorods is completed within 5 min, while lowering the temperature to 200 °C substantially slows down the reaction, without considerably changing the underlying growth mechanism. This allows for capturing the initial growth stages of the particles; what is more, this reaction can be directly compared to the synthesis with high oleic acid concentration described in the next section of the article, because both are conducted at the same temperature.

Transmission electron microscopy (TEM) was used to investigate the shape evolution of CIS NCs. Figure 1 shows TEM images from different stages of the reaction with a low

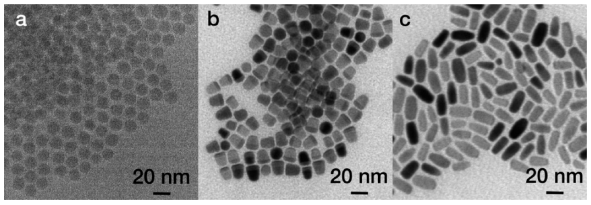

Figure 1. Overview TEM images of particles obtained in reaction with 10 mmol OA at 240 °C; (a) 1 min, (b) 1.5 min, and (c) 5 min.

concentration of OA, conducted at 240 °C, leading to the formation of nanorods. Directly after the injection of the sulfur source, copper sulfide particles form (Figure 1a). In the next step, a second phase appears on one side of the copper sulfide particles (TEM image in Figure 1b, HRTEM images in Supporting Information Figure S1). Spatially resolved EDX measurements (Supporting Information Figure S2) confirm that the emerging phase is copper indium sulfide. The XRD pattern of this sample can be assigned to the wurtzite structure of $CuInS_2$ (see Supporting Information Figure S3). The hybrid NCs have a length of 16.23 ± 1.3 nm and a diameter of 13.4 ± 1.6 nm (Figure 1b). The fraction of copper sulfide within these hybrid nanoparticles is relatively small; furthermore, we expect substantial broadening of the respective XRD reflections. This makes reliable determination of the crystallographic structure of this phase from the XRD data impossible (see XRD pattern in Supporting Information Figure S3). Five minutes after the injection of the thiols, the biphasic structure is converted to monophasic CIS nanorods with a length of 25.15 ± 3.0 nm (Figure 1c). These particles do not grow further, even if they are kept at 240 °C for another 1 h. Their stoichiometry is $CuInS_{2.5}$, which is close to the value expected for copper indium disulfide. The excess sulfur probably originates from thiols present on the surface of the nanorods.

The crystallographic structure of the monophasic CIS nanorods was investigated by powder X-ray diffraction (XRD). The Rietveld refinement of the XRD pattern using an anisotropic size-strain model[28] reveals that the particles have a wurtzite structure, and their preferential growth direction is along the *c* axis (Figure 2).

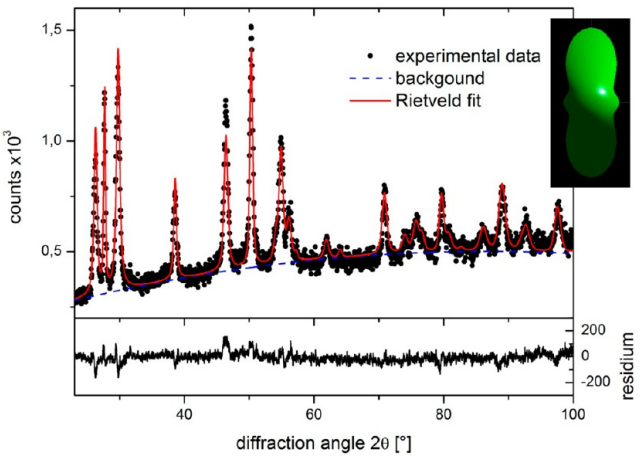

Figure 2. XRD pattern of nanorods obtained in reaction with 10 mmol OA at 240 °C after 5 min together with the results of Rietveld refinement of this pattern using an anisotropic size-strain model developed by Popa.[28] The inset shows the shape model resulting from the Rietveld analysis.

Absorption spectra of particles obtained at different reaction time are shown in Figure 3. The featureless absorption spectrum of the first aliquot taken from the reaction solution (red curve in Figure 3), containing only copper sulfide particles, is characteristic of the prevailing indirect semiconductor. The spectrum of the aliquot taken 1.5 min after the injection (green curve in Figure 3) shows already a shoulder around 750 nm, which is typical for CIS NCs. The fraction of copper sulfide in the sample is relatively small; furthermore, CIS and copper sulfide both absorb light in the same spectral region. Therefore,

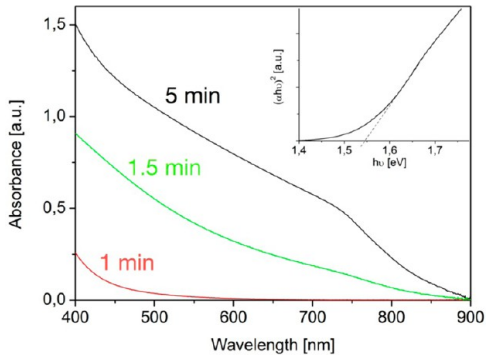

Figure 3. UV–vis absorption spectra of particles resulting from a reaction with 10 mmol OA at 240 °C at different reaction time. The inset shows a Tauc plot for the nanorods obtained at a reaction time of 5 min.

we cannot identify the contribution of the copper sulfide part of the hybrid nanostructure in the absorption spectrum in a reliable way. Because of the relatively large size of CIS NCs compared to the Bohr exciton radius of CIS (4 nm),[29] we do not expect to observe a size quantization effect for this sample. Indeed, the optical band gap (determined from a Tauc plot with $n = 2$ for a direct allowed transition) is 1.54 eV, which matches well the value for the bulk material. The optical band gap does not change as the growth continues, and biphasic nanorods are converted to pure CIS (Tauc plot in the inset in Figure 3).

In contrast to the reaction conducted at 240 °C with 10 mmol oleic acid, during the reaction taking place at 200 °C (with the same composition of the reaction solution) the formation of copper sulfide seeds occurs 15 min after the injection of the thiols. These seeds are relatively large; their diameter is 8.0 ± 1.8 nm (Figure 4a). The formation of CIS

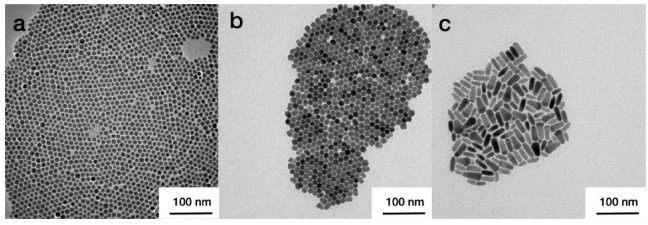

Figure 4. Overview TEM images of different growth stages of particles obtained in reactions with 10 mmol OA at 200 °C; (a) 15 min, (b) 30 min, and (c) 60 min.

within these seeds starts 20 min after the injection of the thiols, and, at a reaction time of 30 min, hybrid nanostructures composed of copper sulfide and CIS can be observed. These particles, forming well ordered assemblies on the TEM grid (Figure 4b), have a relatively uniform diameter of 12 ± 1.4 nm and a length of 21.8 ± 2.6 nm. The hybrid nanostructures grow longer during the further reaction and reach a length of 29 ± 10 nm after 1 h, while their mean thickness does not change (Figure 4c).

The samples taken at different reaction time from this reaction solution were studied by powder X-ray diffraction, in order to elucidate the crystallographic structure of the copper sulfide seeds and of both phases comprising the hybrid nanoparticles. Hybrid nanoparticles containing a relatively high fraction of copper sulfide could be investigated here,

dx.doi.org/10.1021/am5061454 | ACS Appl. Mater. Interfaces 2014, 6, 20535–20543

because of their slow growth process at 200 °C. The sample taken at a reaction time of 15 min (Figure 5b) contains a

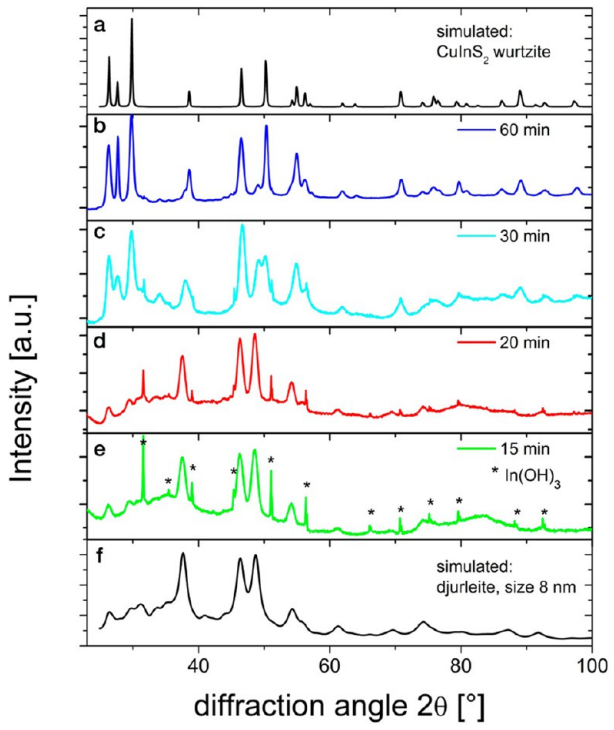

Figure 5. XRD patterns of nanoparticles obtained in a reaction with 10 mmol OA at 200 °C at different reaction times, 15 min (e), 20 min (d), 30 min (c), and 60 min (b), together with simulated patterns for djurleite (f) and wurtzite CIS (a).

considerable fraction of $In(OH)_3$ formed in a reaction between indium(III) acetate and oleylamine.[12] The reflections corresponding to this compound can be found also in aliquots taken at longer reaction time (20 and 30 min, Figure 5c and d), however, with a lower intensity, indicating that it is used up during the further reaction.

An unambiguous assignment of the crystallographic structure of copper sulfide particles based on X-ray diffraction data is not possible in many cases.[7] The diffraction patterns of djurleite and low chalcocite are difficult to distinguish, especially if the reflections are broadened due to the small size of the crystallites. Therefore, djurleite nanocrystals were sometimes misassigned as chalcocite.[7,30] It has to be noted, however, that chalcocite is only stable under air free conditions, while Cu_2S nanocrystals handled under air undergo a phase transition to djurleite. Therefore, we expect our samples, which were exposed to air after the synthesis, to contain djurleite rather than chalcocite nanocrystals. The diffraction pattern of the copper sulfide particles (Figure 5e) can be assigned indeed to this structure; there is a good agreement between the measured pattern and the one simulated for 8 nm djurleite particles (Figure 5f). Because it is not possible to unambiguously assign the crystallographic structure of copper sulfide to one of this both phases (djurleite and low chalcocite) based on X-ray diffraction data, we also measured the composition of the particles by EDX. The resulting stoichiometry, $Cu_{1.9}S$, corroborates our assignment of the crystallographic structure to the copper deficient djurleite phase.

Also the sample taken 20 min after the injection of the thiols contains copper sulfide particles with djurleite structure, while the formation of the wurtzite CIS phase can be observed in the aliquot taken at a reaction time of 30 min (Figure 5c). In the diffraction pattern of these particles, the contribution of both phases can be detected. The intensity of the reflections corresponding to the djurleite phase decreases during the further growth of the hybrid nanostructures (Figure 5b). This is in agreement with the TEM results, showing that the fraction of the copper sulfide phase becomes smaller within the hybrid nanocrystals with longer reaction time (Figure 4c).

The structure of the hybrid nanoparticles was also studied by high resolution TEM (Figure 6a). A closer look at the

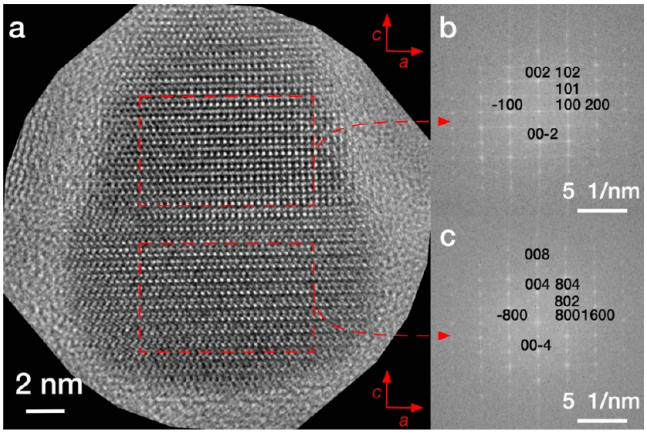

Figure 6. HRTEM image of a hybrid nanoparticle obtained in a reaction with 10 mmol OA at 200 °C at a reaction time of 30 min (a) and the FFTs of the lower (b) and upper (c) part of this particle, consisting of CIS and copper sulfide, respectively. For the sake of clarity, only a few reflections are indexed in the FFT patterns, which can be assigned to wurtzite CIS and djurleite, both viewed along the ⟨010⟩ axis of the respective crystallographic structure.

nanoparticles reveals that the orientation of both parts forming the hybrid nanostructure is not random. The long axis of the hybrid nanorods is parallel to the *c* axis of both the CIS and copper sulfide part of the nanostructure, as can be seen from the FFT patterns in Figure 6b and c.

3.2. Formation of CIS Nanorods and Networks Starting with In Situ Formed 4-nm Copper Sulfide Seeds. Increasing the amount of OA substantially speeds up the formation of the seeds (in comparison to the experiment conducted at 200 °C with 10 mmol OA). In reactions with 50 mmol OA, we observe the formation of copper sulfide particles already 1 min after the injection of the sulfur source. It has to be noted that the overall concentration of the monomers is lower in this reaction, which should increase the critical radius, compared to the synthesis conducted with 10 mmol OA. However, the seeds formed here are smaller than the ones obtained in reactions described in Section 3.1, which suggests that other effects than the dilution affect their size (see Section 3.3). Their diameter increases during the further reaction and reaches 3.9 ± 0.7 nm at a reaction time of 3 min (Figure 7a). Because of the small size of these particles resulting in a strong broadening of the XRD pattern (upper panel of Figure 9) and the large variety of different possible copper sulfide phases, we could not determine their crystallographic structure. Only the presence of copper thiolate (forming a layered structure yielding a characteristic XRD pattern), which is difficult to separate from the copper sulfide seeds during the standard cleaning procedure, could be confirmed by analyzing the

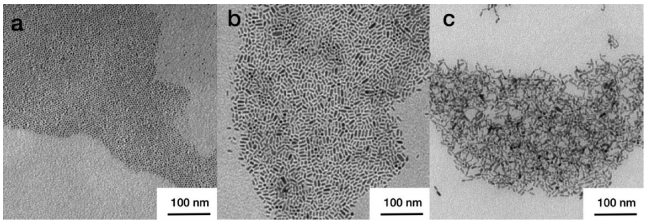

Figure 7. Overview TEM images of different growth stages of particles obtained in reactions with 50 mmol OA at 200 °C; (a) 3 min, (b) 10 min, and (c) 60 min.

diffraction pattern of this aliquot (upper panel of Figure 9). In the next step, the seeds grow to form short nanorods, which subsequently grow longer and reach a length of 8.8 ± 2.9 nm 10 min after the injection (Figure 7b). Their diameter, which is 4.5 ± 1.2 nm, corresponds to the diameter of the copper sulfide seeds. In contrast to the reaction conducted with a low oleic acid concentration, hybrid nanostructures cannot be found at any stage of this reaction; no phase boundaries can be observed (Figure 8a). The analysis of the high resolution TEM

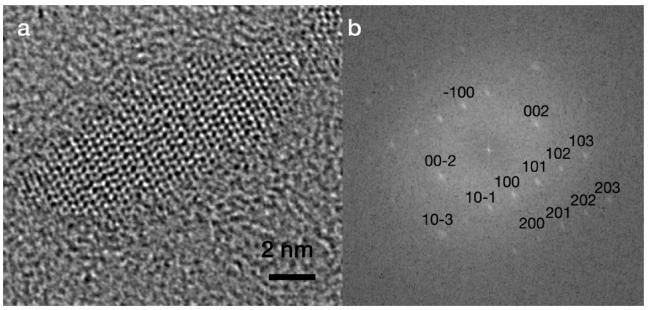

Figure 8. HRTEM image of a nanorod obtained in a reaction with 50 mmol OA at 200 °C at a reaction time of 10 min (a) and the FFT of this particle (b). For the sake of clarity, not all reflections are indexed in this patterns, which can be assigned to wurtzite CIS viewed along the ⟨010⟩ axis.

(HRTEM) images of these nanorods (Figure 8b) and the corresponding XRD pattern (Figure 9) shows that they also

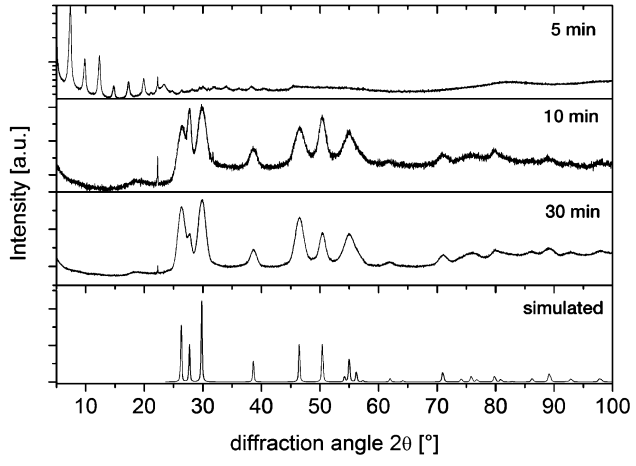

Figure 9. XRD pattern of aliquots taken from the reaction with 50 mmol OA at 200 °C at different reaction times together with a simulated XRD pattern for wurtzite CIS. The sample taken at a reaction time of 5 min containes a large fraction of copper thiolate.

preferentially grow in the direction of the *c* axis of the wurtzite structure. During the growth process of the nanorods, their composition changes from copper rich at a reaction time of 10 min (Cu/In/S 2:1:3.5) to a compound with 1:1:3 stoichiometry at 20 min. Thirty minutes after the injection of the thiols, the particles are indium rich, with a ratio of 1:1.5:4 between copper indium and sulfur. In all cases, the particles are sulfur rich, which we attribute to the presence of thiols in the ligand shell.

Interestingly, when the growth of primary nanoparticles is completed, in reaction with high initial OA concentration they attach together to form multipods (tetrapod-, Y-, and Z-shape particles) and networks of nanorods (Figures 7c and 10). The

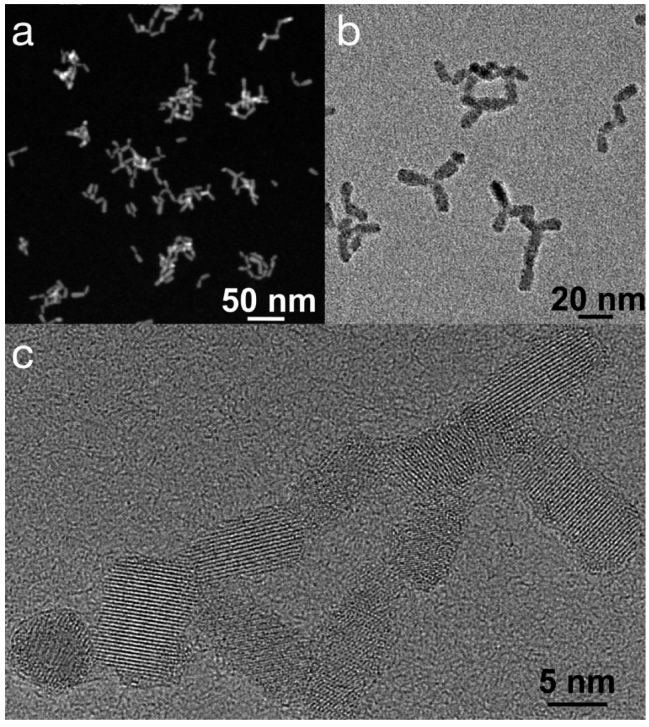

Figure 10. High angle annular dark field (a), TEM (b), and HRTEM (c) images of multipods and small network structures formed by aggregation of nanorods, obtained in reaction with 50 mmol OA at a reaction time of 30 min.

attachment preferentially occurs between the ends of nanorods. However, the structures formed in this manner are composed of randomly oriented primary nanocrystallites and do not form larger single crystals (Figure 10c). Although the nanorods apparently grow together, the sizes of the crystalline domains obtained from the analysis of the X-ray diffraction data in Figure 9 (7 nm perpendicular to the *c*-axis and 11.4 nm parallel to the *c*-axis) do not exceed the sizes of the nanorods forming the multipods and the networks.

The optical band gap determined for the nanorods is 1.64 eV, which is a larger value than the one obtained for the nanorods synthesized with less OA. The thickness of the nanorods is smaller than twice the Bohr exciton radius (8 nm). Thus, the increase of the band gap is most likely due to the quantum size effect. We also do not observe a change in the optical band gap after the formation of the networks (Figure 11), which is in agreement with fact that the aggregation does not lead to an increase of the size of the crystalline domaines.

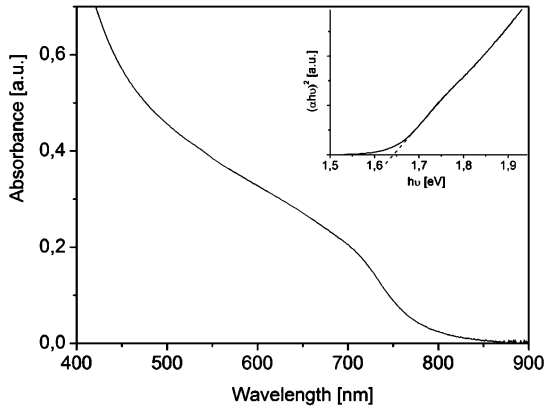

Figure 11. UV−vis absorption spectra of the networks resulting from a reaction with 50 mmol OA at 200 °C at a reaction time of 30 min. The inset shows the Tauc plot (with $n = 2$ for an allowed direct transition) for this absorption spectrum.

The formation of aggregates suggests a weak stabilization of the surface of primary nanorods.[31] Thus, it is surprising, at the first glance, that an increase of the OA amount in the reaction solution has induced the aggregation of the nanorods. Higher concentration of ligands should lead to a more effective passivation of the surface of the NCs and, consequently, prevent their aggregation. Another question arising from the comparison of the reactions with different OA concentration is the reason for the difference of the growth process and the presence of intermediates containing copper sulfide only in reactions with the low OA concentration.

3.3. NMR Investigation of the Reaction Solution. In order to elucidate the factors responsible for the differences in the growth process in reactions with different oleic acid concentrations, we studied the composition of both reaction solutions during the reaction process with ^{1}H and ^{13}C nuclear magnetic resonance (NMR) spectroscopy. The assignment of the peaks, described below, was done by comparison with measured spectra of OA and OLAM, as well as with simulated spectra shown in the Supporting Information (Figure S4−S7).

In the ^{1}H NMR spectrum of the aliquot taken directly before the injection of the thiols from the reaction solution with low oleic acid concentration, no signals stemming from protons next to the functional groups of oleylamine or oleic acid can be detected (lowest panel in Figure 12a). This is due to the presence of the paramagnetic Cu^{2+} ions (because of the partial oxidation of the Cu(I) acetate handled under air), which reduce the spin−spin relaxation time of the protons in their vicinity. The absence of any signal from these protons in spite of the relatively large ratio between the solvent and metal ions suggests a fast exchange dynamics in the metal oleylamin (or oleic acid) complexes. In the reaction solution containing more OA, strongly broadened signals can be detected at 1.7 and 2.8 ppm, which can be assigned to the $-C\mathbf{H}_2-CH_2-NH_2$ and $-CH_2-C\mathbf{H}_2-NH_2$ protons of oleylamine, respectively (lowest panel in Figure 12c).

Thiols can reduce Cu^{2+} to Cu^{+}, therefore, after the injection of 1-DDT and *t*-DDT, the solution does not contain the paramagnetic Cu^{2+} ions. Consequently, the broadening of the signals vanishes, and signals appear, which can be assigned to protons in the vicinity of the carboxylic acid and amino group. Furthermore, peaks at 3.2 and 2.1 ppm are found, which can be assigned to the protons bound to both carbon atoms close to the amid group formed by a reaction of OLAM with oleate or acetate, catalyzed by the presence of metal ions.[12,32−34] OA can protonate acetate ions, and acetic acid forming in this reaction is removed from the solution during the heating process. Therefore, we find the peak related to the $C\mathbf{H}_3-CONH-$ protons only in the reaction solution containing the smaller

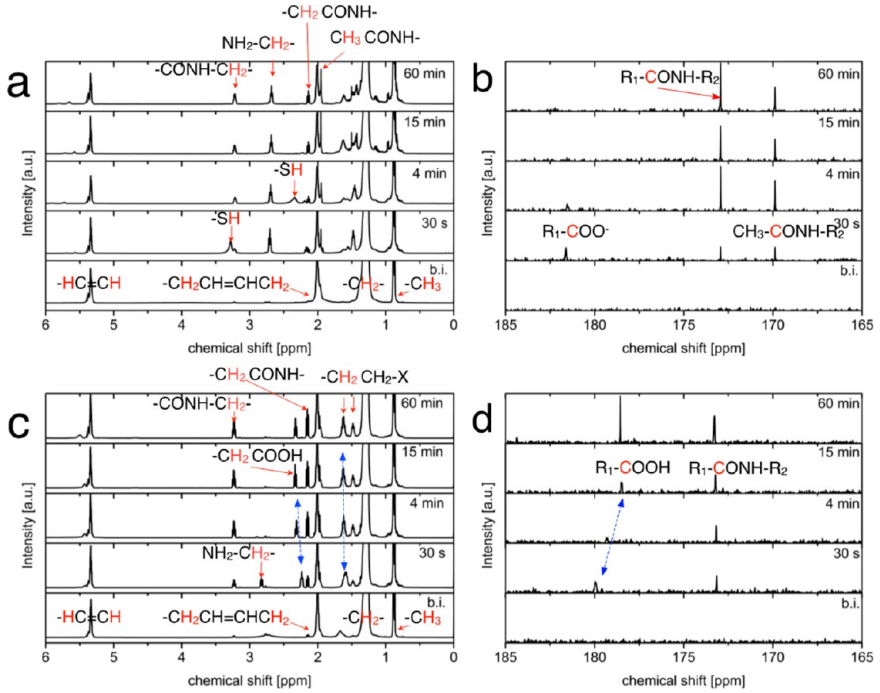

Figure 12. ^{1}H (a, c) and ^{13}C (b, d) NMR spectra of aliquots taken at different reaction times from reactions with 10 mmol OA (a, b) and 50 mmol OA (c, d) at 200 °C, together with the assignment of the signals to the structural elements of organic molecules present in the reaction solutions. R_1-COOH, oleic acid; R_2-NH_2, oleylamine; −X, −COOH, $-NH_2$, or −CONH−; b.i., before injection.

dx.doi.org/10.1021/am5061454 | ACS Appl. Mater. Interfaces 2014, 6, 20535−20543

amount of oleic acid. As pointed out in a recent study on the role of OLAM affecting the precursor conversion, this reaction does not take place at room temperature,[35] however, for our syntheses conducted at 200 °C and above, it influences the stabilization of the nanocrystals and plays a role for their shape control (see below). The signals originating from the amids grow stronger during the further reaction, leading to a complete disappearance of the features, which could be assigned to oleic acid in the reaction with low OA concentration (upper panel in Figure 12a), while, at high OA concentration, the final reaction solution does not contain any OLAM (upper panel in Figure 12c).

Only in the aliquots taken from the solution with a low OA concentration, we observe the presence of free thiols; the peak that can be assigned to the proton of the −SH group is relatively broad and can be found between 3.3 and 1.5 ppm at various reaction time and, consequently, different composition of the reaction solution. The presence of free −SH groups shows that the cations probably form stable complexes with oleylamine, and these cationic monomers with low activity do not react with thiols easily.

Surprisingly, at the first glance, the monomers present in the reaction solution containing a high concentration of oleic acid are much more reactive and form thiolates already within the first seconds after the injection of the thiols (as can be seen from the lack of a −SH signal in the NMR spectra in Figure 12c). A closer look at the ^{13}C NMR spectra reveals that, for the aliquots taken at 30 s and 4 min, the signal of the carbonyl carbon atom is shifted downfield (indicated by the blue arrow in Figure 12d), compared to the value expected for the −COOH group, indicating the deprotonation of the carboxylic acid by the amine. The $-C\mathbf{H}_2-COOH$ and $-C\mathbf{H}_2-CH_2-COOH$ protons are shifted upfield for these two samples (indicated by blue arrows in Figure 12 c), which is expected if the carboxylic group is deprotonated. The shift in ^{13}C and ^{1}H NMR spectra related to the formation of carboxylates gradually becomes smaller and vanishes within several minutes of the reaction. This is due to the decrease of the OLAM concentration in the reaction solution (at the same time the signals that can be assigned to OLAM disappear). The formation of carboxylate and amino ions in the reaction solution containing comparable amounts of oleic acid and oleylamine, is the reason for the higher activity of the cationic monomers. It reduces the concentration of OA and OLAM available for the coordination of the cations, which results in a higher activity of the cationic monomers, compared to that in the solution containing less OA.

Thus, OA influences the reactivity of the monomers in this reaction in an indirect manner, by protonating OLAM. The increase of the activity of the monomers achieved in this way has consequences for the following growth process of the nanocrystals. It leads to a faster formation of copper sulfide seeds in the reaction with higher OA concentration. More importantly, it reduces the critical radius of the stable nuclei in this reaction solution, which leads to the formation of smaller seeds. In such small seeds, there is a substantial contribution of the surface energy, which can strongly influence the phase behavior. It is known from nanocrystalline metal alloys that the formation of alloyed particles is favored for small particle sizes, while phase segregation occurs above a certain critical radius for a given combination of two metals. We assume this effect to be responsible for the altered growth process in the reaction producing smaller copper sulfide seeds. The size of these seeds seems to lie below the critical radius for the phase segregation for the quasi-binary copper sulfide−copper indium disulfide system. This leads to the conversion of the copper sulfide seeds to a copper rich copper indium sulfide compound in the beginning of the reaction, which subsequently incorporates further indium ions into its lattice, until almost stoichiometric copper indium disulfide or even an indium rich compound is formed. Thus, it is possible to obtain CIS starting with small copper sulfide seeds; however, the growth mechanism of the particles changes because of the high surface energy of the small particles.

Finally, the reason for the formation of the networks has to be addressed. The reaction solution contains three compounds, which can stabilize the surface of the nanoparticles: OLAM, OA, and 1-DDT. From the sulfur rich composition of the network nanostructures, we can assume that 1-DDT is present on the surface of the particles. In contrast to this, OA does not seem to be able to stabilize the nanocrystals; formation of networks easily takes place in OA-rich solutions. No aggregation can be observed, when OLAM is present in excess in the reaction solution, which suggests that it is present in the ligand shell. From the fact that we do not observe side-to-side aggregation of the particles, we conclude that OLAM binds to the ends rather than to the sides of the nanorods. Thus, the formation of networks of end-to-end bound nanorods is due to the decreasing stabilizing effect of OLAM, which is gradually removed from the solution by its metal cation catalyzed reaction with OA.

CONCLUSIONS

Applying oleic acid together with oleylamine in the synthesis of semiconductor NCs opens up new possibilities of shape control. Changing the ratio between both compounds influences the reactivity of the cationic monomers in the reaction solution, which, in turn, influences the size of the copper sulfide seeds forming in the first stage of the reaction. Large copper sulfide seeds, forming in solutions of monomers with relatively low activity, play the role of a catalyst for the further growth of CIS nanocrystals. Copper sulfide−copper indium disulfide hybrid nanostructures are intermediates in this kind of reactions. When the seeds are small, a gradual conversion of copper sulfide into copper indium disulfide is observed, rather than a phase separation, because of the contribution of the surface energy substantially influencing the phase behavior.

Furthermore, the reaction between OA and OLAM to an amide leads to a gradual destabilization of the NCs during the reaction. This induces a secondary growth by an attachment mechanism and a formation of CIS NCs with new shapes, such as multipods and networks. These structures are of particular interest in view of their potential application in photovoltaics. Especially in hybrid, organic−inorganic solar cells, the network morphology of the inorganic component should improve the charge transport properties of the active layer. Our strategy, which is based on the reaction between the organic molecules present in the reaction solution, is not limited to CIS but could be also applied to other materials, which can be stabilized by amines or fatty acids.

■ ASSOCIATED CONTENT

Supporting Information

EDX results, additional HRTEM images, XRD data, and NMR spectra. This material is available free of charge via the Internet at http://pubs.acs.org.

■ AUTHOR INFORMATION

Corresponding Author

*E-mail: joanna.kolny@uni-oldenburg.de.

Author Contributions

The manuscript was written through contributions of all authors.

Notes

The authors declare no competing financial interest.

■ ACKNOWLEDGMENTS

We gratefully acknowledge funding of the EWE Research Group "Thin Film Photovoltaics" by the EWE AG, Oldenburg.

■ REFERENCES

(1) Alivisatos, P. Perspectives on the Physical Chemistry of Semiconductor Nanocrystals. *J. Phys. Chem.* **1996**, *100*, 13226−13239.

(2) Weller, H. Kolloidale Halbleiter-Q-Teilchen: Chemie im Übergangsbereich zwischen Festkörper und Molekül. *Angew. Chem.* **1993**, *105*, 43−55.

(3) Burda, C.; Chen, X.; Narayanan, R.; El-Sayed, M. A. Chemistry and Properties of Nanocrystals of Different Shapes. *Chem. Rev.* **2005**, *105*, 1025−1102.

(4) Yu, K.; Hrdina, A.; Ouyang, J.; Kingston, D.; Wu, X.; Leek, D. M.; Liu, X.; Li, C. Ultraviolet $ZnSe_{1-x}S_x$ Gradient-Alloyed Nanocrystals via a Noninjection Approach. *ACS Appl. Mater. Interfaces* **2012**, *4*, 4302−4311.

(5) Yu, K.; Ng, P.; Ouyang, J.; Badruz Zaman, M.; Abulrob, A.; Baral, T. N.; Fetehi, D.; Jakubek, Z. J.; Kingston, D.; Wu, X.; Liu, X.; Hebert, C.; Leek, D. M.; Whitfield, D. M. Low-Temperature Approach to Highly Emissive Copper Indium Sulfide Colloidal Nanocrystals and their Bioimaging Applications. *ACS Appl. Mater. Interfaces* **2013**, *5*, 2870−2880.

(6) Talapin, D. V.; Lee, J.-S.; Kovalenko, M. V.; Shevchenko, E. V. Prospects of Colloidal Nanocrystals for Electronic and Optoelectronic Applications. *Chem. Rev.* **2010**, *110*, 389−458.

(7) Zhao, Y.; Burda, C. Development of Plasmonic Semiconductor Nanomaterials with Copper Chalcogenides for a Future with Sustainable Energy Materials. *Energy Environ. Sci.* **2012**, *5*, 5564−5576.

(8) Zhong, H.; Bai, Z.; Zou, B. Tuning the Luminescence Properties of Colloidal I−III−VI Semiconductor Nanocrystals for Optoelectronics and Biotechnology Applications. *J. Phys. Chem. Lett.* **2012**, *3*, 3167−3175.

(9) Kolny-Olesiak, J.; Weller, H. Synthesis and Application of Colloidal $CuInS_2$ Semiconductor Nanocrystals. *ACS Appl. Mater. Interfaces* **2013**, *5*, 12221−12237.

(10) Aldakov, D.; Lefrançois, A.; Reiss, P. Ternary and Quaternary Metal Chalcogenide Nanocrystals: Synthesis, Properties, and Applications. *J. Mater. Chem. C* **2013**, *1*, 3756−3776.

(11) Connor, S. T.; Hsu, C.-M.; Weil, B. D.; Aloni, S.; Cui, Y. Phase Transformation of Biphasic Cu_2S-$CuInS_2$ to Monophasic $CuInS_2$ Nanorods. *J. Am. Chem. Soc.* **2009**, *131*, 4962−4966.

(12) Kruszynska, M.; Borchert, H.; Parisi, J.; Kolny-Olesiak, J. Investigations of Solvents and Various Sulfur Sources Influence on the Shape-Controlled Synthesis of $CuInS_2$ Nanocrystals. *J. Nanopart. Res.* **2011**, *13*, 5815−5824.

(13) Kruszynska, M.; Borchert, H.; Parisi, J.; Kolny-Olesiak, J. Synthesis and Shape Control of $CuInS_2$ Nanoparticles. *J. Am. Chem. Soc.* **2010**, *132*, 15976−15986.

(14) Lu, X.; Zhuang, Z.; Peng, Q.; Li, Y. Controlled Synthesis of Wurtzite $CuInS_2$ Nanocrystals and their Side-by-Side Nanorod Assemblies. *CrystEngComm* **2011**, *13*, 4039−4045.

(15) Wang, L.-W. High Chalcocite Cu_2S: A Solid−Liquid Hybrid Phase. *Phys. Rev. Lett.* **2012**, *108*, 085703.

(16) Kolny-Olesiak, J. Synthesis of Copper Sulphide-Based Hybrid Nanostructures and their Application in Shape Control of Colloidal Semiconductor Nanocrystals. *CrystEngComm* **2014**, *16*, 9381−9390.

(17) Han, S.-K.; Gong, M.; Yao, H.-B.; Wang, Z.-M.; Yu, S.-H. One-Pot Controlled Synthesis of Hexagonal-Prismatic $Cu_{1.94}S$−ZnS, $Cu_{1.94}S$−ZnS−$Cu_{1.94}S$, and $Cu_{1.94}S$−ZnS−$Cu_{1.94}S$−ZnS−$Cu_{1.94}S$ Heteronanostructures. *Angew. Chem., Int. Ed.* **2012**, *51*, 6365−6368.

(18) Yi, L.; Tang, A.; Niu, M.; Han, W.; Hou, Y.; Gao, M. Synthesis and Self-Assembly of $Cu_{1.94}S$−ZnS Heterostructured Nanorods. *CrystEngComm* **2010**, *12*, 4124−4130.

(19) Chang, J.-Y.; Cheng, C.-Y. Facile One-Pot Synthesis of Copper Sulfide−Metal Chalcogenide Anisotropic Heteronanostructures in a Noncoordinating Solvent. *Chem. Commun.* **2011**, *47*, 9089−9091.

(20) Coughlan, C.; Singh, A.; Ryan, K. Systematic Study into the Synthesis and Shape Development in Colloidal $CuIn_xGa_{1-x}S_2$ Nanocrystals. *Chem. Mater.* **2013**, *25*, 653−661.

(21) Li, Q.; Zhai, L.; Zou, C.; Huang, X.; Zhang, L.; Yang, Y.; Chen, X.; Huang, S. Wurtzite $CuInS_2$ and $CuIn_xGa_{1-x}S_2$ Nanoribbons: Synthesis, Optical and Photoelectrical Properties. *Nanoscale* **2013**, *5*, 1638−1648.

(22) Liao, H.-C.; Jao, M.-H.; Shyue, J.-J.; Chen, Y.-F.; Su, W.-F. Facile Synthesis of Wurtzite Copper−Zinc−Tin Sulfide Nanocrystals from Plasmonic Djurleite Nuclei. *J. Mater. Chem. A* **2013**, *1*, 337.

(23) Zhang, W.; Zhai, L.; He, N.; Zou, C.; Geng, X.; Cheng, L.; Dong, Y.; Huang, S. Solution-Based Synthesis of Wurtzite Cu_2ZnSnS_4 Nanoleaves Introduced by α-Cu_2S Nanocrystals as a Catalyst. *Nanoscale* **2013**, *5*, 8114−8121.

(24) Zhou, J.; Huang, F.; Xu, J.; Wang, Y. $Cu_{1.94}S$−MnS Dimeric Nanoheterostructures with Bifunctions: Localized Surface Plasmon Resonance and Magnetism. *CrystEngComm* **2013**, *15*, 4217−4220.

(25) Kruszynska, M.; Borchert, H.; Bachmatiuk, A.; Rümmeli, M. H.; Buechner, B.; Parisi, J.; Kolny-Olesiak, J. Size and Shape Control of Colloidal Copper (I) Sulfide Nanorods. *ACS Nano* **2012**, *6*, 5889−5896.

(26) Kruszynska, M.; Parisi, J.; Kolny-Olesiak, J. Synthesis and Shape Control of Copper Tin Sulphide Nanocrystals and Formation of Gold−Copper Tin Sulphide Hybrid Nanostructures. *Z. Naturforsch.* **2014**, *69a*, 446−450.

(27) Xie, R.; Rutherford, M.; Peng, X. Formation of High-Quality I-III-VI Semiconductor Nanocrystals by Tuning Relative Reactivity of Cationic Precursors. *J. Am. Chem. Soc.* **2009**, *131*, 5691−5697.

(28) Popa, N. The (*hkl*) Dependence of Diffraction-line Broadening Caused by Strain and Size for all Laue Groups in Rietveld Refinement. *J. Appl. Crystallogr.* **1998**, *31*, 176−180.

(29) Zhong, H.; Zhou, Y.; Ye, M.; He, Y.; Ye, J.; He, C.; Yang, C.; Li, Y. Controlled Synthesis and Optical Properties of Colloidal Ternary Chalcogenide $CuInS_2$ Nanocrystals. *Chem. Mater.* **2008**, *20*, 6434−6443.

(30) Zhao, Y.; Pan, H.; Lou, Y.; Qiu, X.; Zhu, J.; Burda, C. Plasmonic $Cu_{2-x}S$ Nanocrystals: Optical and Structural Properties of Copper-Deficient Copper(I) Sulfides. *J. Am. Chem. Soc.* **2009**, *131*, 4253−4261.

(31) Penn, R. Kinetics of Oriented Aggregation. *J. Phys. Chem. B* **2004**, *108*, 12707−12712.

(32) Jin, X.; Li, J.; Parisi, J.; Kolny-Olesiak, J. Shape Control of CdTe Nanocrystals Synthesized in Presence of In Situ Formed CdO Particles. *J. Nanopart. Res.* **2011**, *13*, 6963−6970.

(33) Jin, X.; Kruszynska, M.; Parisi, J.; Kolny-Olesiak, J. Catalyst-free Synthesis and Shape Control of CdTe Nanowires. *Nano Res.* **2011**, *4*, 824−835.

(34) Selishcheva, E.; Parisi, J.; Kolny-Olesiak, J. Copper-Assisted Shape Control in Colloidal Synthesis of Indium Oxide Nanoparticles. *J. Nanopart. Res.* **2012**, *14*, 711.

(35) Yu, K.; Liu, X.; Chen, Q. Y.; Yang, H.; Yang, M.; Wang, X.; Wang, X.; Cao, H.; Whitfield, D. M.; Hu, C.; Tao, Y. Mechanistic Study of the Role of Primary Amines in Precursor Conversions to Semiconductor Nanocrystals at Low Temperature. *Angew. Chem., Int. Ed. Engl.* **2014**, *53*, 6898−6904.